X-ray selection of Compton Thick AGN at high redshift

G. Lanzuisi[1,2,⋆]

[1] Dipartimento di Fisica e Astronomia, Universitá degli studi di Bologna, Via Ranzani 1, 40127, Bologna, Italy
[2] INAF-Osservatorio Astronomico di Bologna, Via Ranzani 1, 40127, Bologna, Italy

Received 2016 Sep 23, accepted 2016 Oct 24
Published online later

Key words galaxies: active – X-rays: galaxies

Compton Thick (CT) AGN are a key ingredient of Cosmic X-ray Background (CXB) synthesis models, but are still an elusive component of the AGN population beyond the local Universe. Multiwavelength surveys are the only way to find them at $z \gtrsim 0.1$, and a deep X-ray coverage is crucial in order to clearly identify them among star forming galaxies. As an example, the deep and wide COSMOS survey allowed us to select a total of 34 CT sources. This number is computed from the 64 nominal CT candidates, each counted for its N_H probability distribution function. For each of these sources, rich multiwavelength information is available, and is used to confirm their obscured nature, by comparing the expected AGN luminosity from spectral energy distribution fitting, with the absorption-corrected X-ray luminosity. While *Chandra* is more efficient, for a given exposure, in detecting CT candidates in current surveys (by a factor ~ 2), deep *XMM–Newton* pointings of bright sources are vital to fully characterize their properties: N_H distribution above 10^{25} cm^{-2}, reflection intensity etc., all crucial parameters of CXB models. Since luminous CT AGN at high redshift are extremely rare, the future of CT studies at high redshift will have to rely on the large area surveys currently underway, such as XMM-XXL and Stripe82, and will then require dedicated follow-up with *XMM–Newton*, while waiting for the advent of the ESA mission *Athena*.

1 Introduction

We know, since the late 90's, that a large fraction (up to 30%) of local AGN are obscured by large amounts of gas and dust (e.g. Risaliti et al. 1999), above the Compton Thick[1] threshold (CT, $N_H \geq \sigma_T^{-1} \sim 1.5 \times 10^{24}$ cm^{-2}). A similar fraction of CT AGN is required in most Cosmic X-ray Background (CXB) synthesis models (e.g. Comastri et al. 1995, Gilli et al. 2007): their flat spectrum is needed in order to reproduce the hump at 20-30 keV observed in the CXB (e.g. Ballantyne et al. 2011). However, the value of the CT fraction that one can derive is largely uncertain (Treister et al. 2009, Ueda et al. 2014) due to degeneracies between several model parameters, i.e. primary continuum photon index, reflection fraction, N_H distribution above 10^{24} cm^{-2}, and high energy cut-off (see e.g. Akylas et al. 2012).

A population of even more deeply obscured sources ($N_H \geq 10^{25}$ cm^{-2}) may be required (Comastri et al. 2015) in order to reconcile new estimates of the BH mass function in the local Universe (Kormendy & Ho 2015) with that inferred by integrating the luminosity function of observed AGN via the continuity equation (e.g. Soltan 1982; Marconi et al. 2004). These heavily obscured sources, however, will not contribute much to the CXB, since even the highest energy X-rays they produce are blocked by the obscuring material.

Despite their expected large number, CT AGN are very difficult to identify beyond the local Universe, resulting in a small/negligible fraction of CT AGN blindly identified in deep X-ray surveys (e.g. Tozzi et al. 2006, Lanzuisi et al. 2013, Marchesi et al. 2016). Even *NuSTAR*, sensitive above 10 keV, was able to put only upper limits to the fraction of CT AGN at $z = 0.5 - 1$ (Alexander et al. 2013). Therefore, several multiwavelength techniques have been developed in the past decade, based on known CT AGN broad band properties, to pre-select CT AGN beyond the local Universe. IR spectral features, IR colors or mid-IR vs. optical or X-ray flux ratios can be used to select red, dusty sources at $z \sim 2$ (e.g. Lacy et al. 2004, Martinez-Sansigre et al. 2005, Houck et al. 2005). High ionization optical emission lines from the narrow line region, such as [OIII] and [NeV] can be used to select sources with a deficit in the observed X-ray emission, that can be ascribed to strong obscuration of the nucleus (e.g. Vignali et al. 2006, Gilli et al. 2010, Mignoli et al. 2013).

In all these cases, however, the X-ray information (either detections or staking) is crucial in order to unambiguously identify a fraction of CT AGN among inactive galaxies with similar properties (e.g. Fiore et al. 2008, Lanzuisi et al. 2009, Georgantopoulos et al. 2011, Vignali et al. 2014). X-rays are indeed able to provide the smoking gun of the CT nature of these sources, thanks to the unique spectral signatures observable, i.e. the flat continuum and the strong Fe K

⋆ Corresponding author: e-mail: giorgio.lanzuisi2@unibo.it

[1] At these high column densities the obscuration is mainly due to Compton-scattering, rather than photoelectric absorption.

emission line at 6.4 keV. Furthermore, above $L_{\rm X} \sim 10^{42}$ erg s^{-1}, the contamination by star-forming galaxies in the 2-10 keV is limited. Finally, X-ray spectroscopy is favored by the redshift effect: going at high redshift, the Compton hump at 20-30 keV becomes observable by *Chandra* and *XMM–Newton* and the Fe kα line moves toward lower energies, where the effective area of current telescopes is larger.

There are, however, important caveats to take into account: i) The fraction of CT AGN steeply rises from ~ 0 to the intrinsic value (e.g. 0.3-0.4) only below a certain flux (e.g. $F << 10^{-15}$ erg cm^{-2} s^{-1} in the 2-10 keV band) and therefore it is mandatory to reach deep sensitivities, in order to collect sizable samples of CT AGN. ii) CT AGN are a factor 30-50 fainter than normal AGN below 10 keV rest frame, requiring long exposures to collect even few tens of X-ray counts per source. iii) The transition between Compton-thin and Compton-thick is smooth, and the spectra of sources just above/below the CT threshold are very similar (Murphy & Yaqoob 2009), requiring a tailored analysis (see. e.g. Buchner et al. 2015) and possibly the use of the full $N_{\rm H}$ probability distribution function (PDF) when counting/selecting CT AGN, in order to avoid misclassification in one direction or the other.

For all these reasons, even in the deepest X-ray fields, different analysis of the same data sets (e.g. Tozzi et al. 2006, Brightman & Ueda 2012, Georgantopoulos et al. 2013) give different results, not always in agreement (see Castelló-Mor et al. 2013).

Here we present results from the analysis of the large COSMOS-Legacy catalog, that allowed us to select 64 CT AGN candidates among the ~ 4000 point-like sources. For each candidate, the full PDF of the $N_{\rm H}$ is taken into account, to weight each source by its probability of being CT. The LogN-LogS of CT AGN in three redshift bins (up to $z = 3.5$) is also presented.

2 Sample Selection

2.1 The COSMOS survey

The 2 deg^2 area of the *HST* COSMOS Treasury program is centered at 10:00:28.6, +02:12:21.0 (Scoville et al. 2007). The field has a unique deep and wide multi-wavelength coverage, from the optical band (*Hubble, Subaru, VLT* and other ground-based telescopes), to the infrared (*Spitzer, Herschel*), X–ray (*XMM–Newton*, *Chandra* and *NuSTAR*) and radio bands. Large dedicated ground-based spectroscopy programs in the optical with all the major optical telescopes have been completed. Very accurate photometric redshifts are available for both the galaxy population (Ilbert et al. 2009) and the AGN population (Salvato et al. 2011).

The COSMOS field has been observed with *XMM–Newton* for a total of ~ 1.5 Ms at a rather homogeneous depth of $\sim$60 ks over ~ 2 deg^2 (Hasinger et al. 2007, Cappelluti et al. 2009), and by *Chandra* with a deeper observations of ~ 160 ks: the central deg^2 was observed in 2006-2007 (Elvis et al. 2009, Civano et al. 2012) for a total of 1.8 Ms, while addition 1.2 deg^2 were covered recently (2013-2014) by the Chandra COSMOS-Legacy survey, for a total of 2.8 Ms (Civano et al. 2016, Marchesi et al. 2016a).

The *Chandra* catalog used in this work includes 4016 point-like sources (from a total of 4.6 Ms of *Chandra* observation) detected in at least one of the following three bands: full (F; 0.5-7 keV), soft (S; 0.5-2 keV) and hard (H; 2-7 keV). Each source was detected in at least one band with probability of being a spurious detection P$< 2 \times 10^{-5}$.

2.2 X-ray spectral analysis

1949 sources in the COSMOS-Legacy catalog have more than 30 counts (with average ~ 145 and median ~ 68 counts). This threshold allows to derive basic spectral properties ($N_{\rm H}$, $L_{\rm X}$, see Lanzuisi et al. 2013). The result of a systematic spectral analysis of all these sources is presented in Marchesi et al. (2016). The procedure described there, however, is not optimized to look for CT AGN, since at such high column densities, the simple power-law plus photoelectric absorption model does not reproduce any more the physical processes involved.

We reanalyzed all the available spectra using the BNTorus model (Brightman & Nandra 2011), specifically developed to model obscuration at CT regimes. The geometry of the obscuring material is a spherical torus which is essentially a sphere with a bi-conical aperture. We used the model with fixed photon index $\Gamma = 1.9$, and with fixed torus half opening angle (60°) and inclination angle (80°). The model is therefore very simple, as it uses a single geometry and does not allow for any variation between the primary continuum and the reflection/line component, or for different value of $N_{\rm H}$ between the absorber and the reflector[2]. However this choice is forced by the very limited number of counts available for each source (65% of the final CT sample has less than 50 net counts). In addition to the BNTorus model, we used a secondary powerlaw, with the photon index fixed to 1.9, to model the emission emerging in the soft band in most of the obscured spectra (Lanzuisi et al. 2015a). The normalization of this component is forced to be $< 10\%$ of the primary component.

Once the best fit is obtained, we run a Monte Carlo Markov Chain (MCMC) within *Xspec* (v. 12.8.2), to evaluate the $N_{\rm H}$ probability distribution function (PDF). In this way we can collect a sample of CT AGN candidates, by counting each source that is close to the CT boundary, only for the part of the PDF that exceeds this boundary. Fig. 1 and 2 show the unfolded spectra and residuals for two CT AGN selected in this way. The bottom panels show the $N_{\rm H}$ PDF (in red the part of the PDF that is taken into account to weight the source). Thanks to this analysis we were able to select a sample of 64 obscured sources, at $0.04 < z < 3.46$,

[2] as e.g. MYTorus in the decoupled version is able to do (Murphy & Yaqoob 2009).

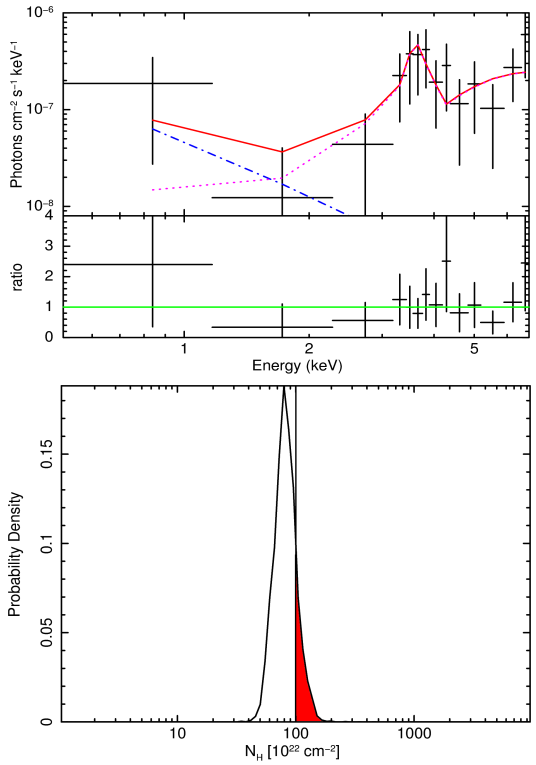

Fig. 1 *Top:* Unfolded spectrum and data-to-model ratio of the CT candidate LID_633 at $z = 0.706$. In magenta is shown the BNtorus component, in blue the soft powerlaw, and in red the total. *Bottom:* PDF of N_H for the spectrum shown above.

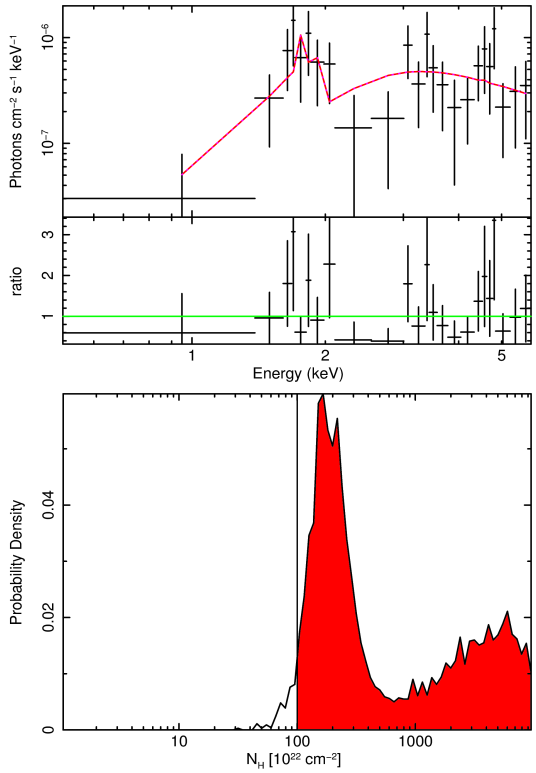

Fig. 2 *Top:* Unfolded spectrum and data-to-model ratio of the CT candidate LID_1002 at $z = 2.612$. This source only required the BNtorus component. *Bottom:* PDF of N_H for the same source.

having $> 5\%$ probability of being CT (i.e. a fraction of them is not nominally CT). Summing up only the fraction of the PDF of each source that is above 10^{24} cm^{-2}, we obtained a number of CT sources of $N_{CT} = 33.85$.

3 Results

The sample of selected CT candidates spans a wide range in redshift, $0.04 < z < 3.46$ (50% of them have a photometric redshift) and absorption corrected X-ray luminosity, $43.5 <$Log(L_X)< 45.8 erg s^{-1}, with the exception of source LID_1791 having Log(L_X)$= 42.2$ erg s^{-1}at z=0.04, identified as a CT AGN in Civano et al. (2015)[3].

Given the large correction applied due to the obscuration, almost all the sources in the sample are in the quasar regime ($L_X > 10^{44}$ erg s^{-1}, see blue points in fig. 3). In order to verify if these luminosities are reasonable, and therefore if our estimate of the obscuration is correct and not overestimated, we verified that the X-ray luminosity derived after correcting for the obscuration is consistent, within ~ 1 dex with the mid-IR AGN luminosity as computed from the spectral energy distribution (SED) fitting (either from Delvecchio et al. 2015 or Suh et al. 2016), after removing the host star-formation emission. Fig. 3 shows the distribution of the AGN Mid-IR ($6\mu m$) luminosity, vs. the absorption-corrected L_X, for the ~ 2000 sources analyzed in Marchesi et al. 2016 (gray crosses). Red circles show the observed L_X of the CT candidates, while blue circles show the absorption-corrected L_X.

Almost all our CT AGN have their $L_{6\mu m}$-L_X within the typical scatter from the average relation (the orange or green curves, the $L_{6\mu m}$-L_X relations published in Gandhi et al. 2009 and Stern 2015, respectively). However the vast majority lie in the upper part of the distribution: this is a clear selection effect (see e.g. Lanzuisi et al. 2015a) due to the fact that CT sources with intrinsic L_X in the lower part of the diagram would have not been detected in X-rays, having an absorbed L_X (and hence flux) below the detection threshold of the survey. This already tells us that, despite our effort, a sizable fraction of CT AGN is still missing due to their low X-ray fluxes.

3.1 LogN-LogS

To overcome this incompleteness, we can look at the LogN-LogS distribution, where we can compare CXB models with the number of sources detected above the flux threshold of the survey. To investigate a possible variation of the CT fraction with redshift, we divided the sample into three redshift

[3] This source is one of the two, with LID_633, that is detected with *NuSTAR*. The N_H values are consistent between our fit and the ones performed using also the hard X-ray data (Zappacosta et al. 2016 in prep.).

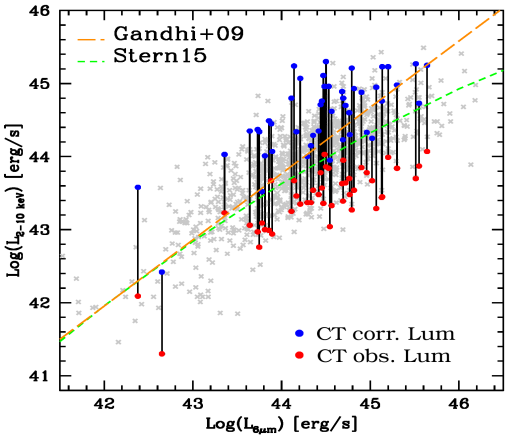

Fig. 3 Distribution of the AGN Mid-IR ($6\mu m$) luminosity, as derived from SED fitting, after subtracting the host star-formation emission, and the 2-10 keV luminosity, for the $\sim$ 2000 sources analyzed in Marchesi et al. 2016 (gray crosses). Red circles show the observed $L_{\rm X}$ for the CT candidates, while blue circles show the absorption-corrected $L_{\rm X}$. The orange (green) curve shows the relation published in Gandhi et al. 2009 (Stern 2015).

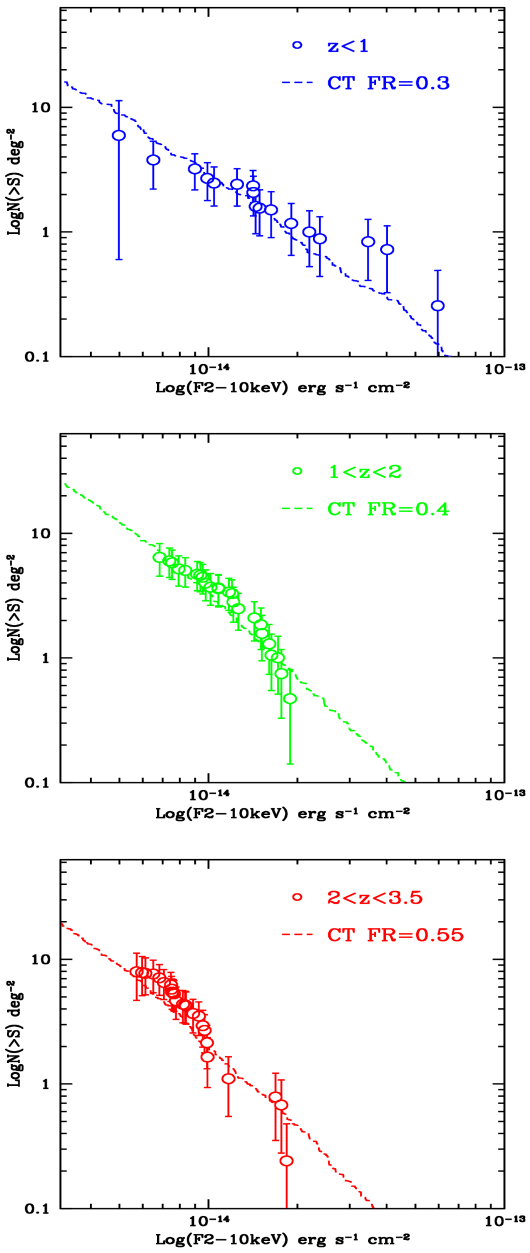

Fig. 4 Observed LogN-LogS of CT candidates at $z < 1$ (top), $1 < z < 2$ (center) and $2 < z < 3.5$ (bottom), compared with the model for Akylas et al. 2012, with different CT fractions (FR).

bins, and compared the observed LogN-LogS, with the one predicted from the Akylas et al. (2012) model (Fig. 4). This model assumes $\Gamma = 1.9$, a high energy cut-off of 195 keV and a fraction of the reflected component flux with respect to the primary powerlaw of 0.05 in the 2-10 keV band. To match the observed LogN-LogS of the CT AGN selected in COSMOS, the fraction of sources in the Log(N_H) bins 24-26 (equally distributed between the 24-25 and 25-26 bin) must increase, from 30% in the $z < 1$ bin, to 40% in the $1 < z < 2$, up to 55% in the $2 < z < 3.5$ bin. These fractions are systematicly higher than what predicted from other CXB models such as the one of Gilli et al. (2007) and Treister et al. (2009).

Brightman & Ueda (2012) have already found a hint of an increase of the CT fraction from $z < 0.1$ (20% derived in Burlon et al. 2011) to $z > 1$ (40% based on only 8 sources), while other authors have found no evolution of the CT fraction at high z (e.g. Buchner et al. 2015). We confirm the increase in the fraction of CT, especially at $2 < z < 3.5$, with a sample of 24 sources, (the sum of all the probability distributions gives $\sim$ 13 sources). This result is in agreement with the idea that at, high redshift, other factors, such as the concentration of dense gas and dust clouds in the central region of the host galaxy (possibly induced by gas-rich mergers), may contribute to CT obscuration, on top of the canonical molecular torus (e.g. Hopkins et al. 2006).

3.2 Extremely obscured CT

Of particular interest is the observed distribution of N_H above 10^{25} cm^{-2}, first of all because it is mostly unknown, even at low redshift (see e.g. Maiolino et al. 2003), and second because it is not possible to derive any estimate on the number of heavily CT sources with the indirect method of the CXB synthesis models.

Very few (e.g. Piconcelli eta l. 2011, Gandhi et al. 2013, or the debated case of Arp220, Wilson et al. 2014) of these reflection dominated sources is known in the local universe (see the compilation of Gandhi et al. 2014), and even more uncertain is their fraction above z$\sim$ 0.1.

In Lanzuisi et al. (2015b) we have found the first N_H= 10^{25} cm^{-2} CT AGN candidate in COSMOS, thanks to several multiwavelength indicators ([NeV], IR and bolometric luminosity from SED). With the analysis presented here we

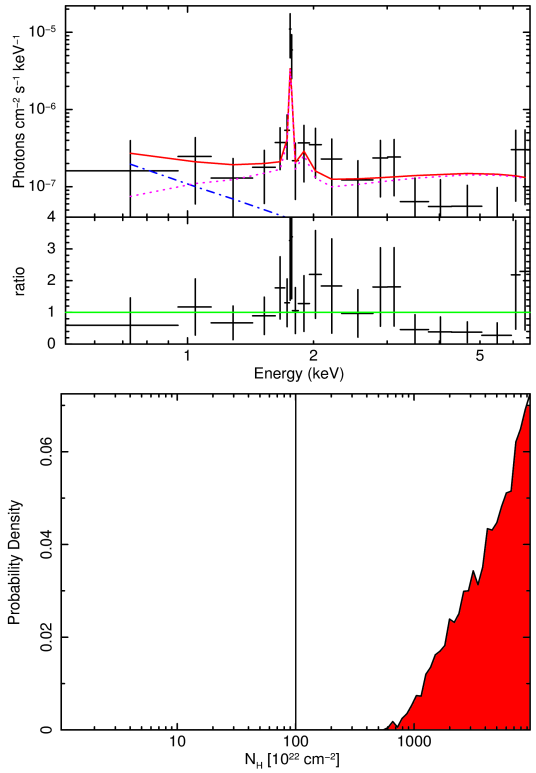

Fig. 5 *Top:* Unfolded spectrum and data-to-model ratio of the heavily CT candidate CID_708. *Bottom:* PDF of N_H for the same source.

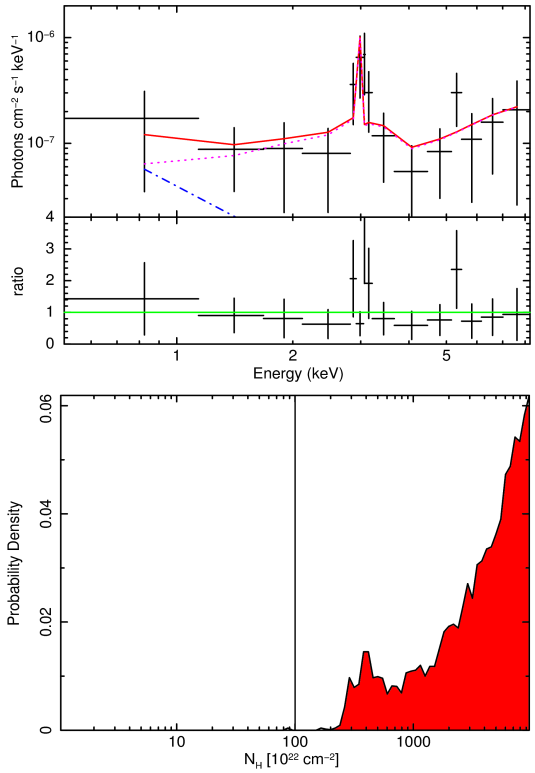

Fig. 6 As fig. 5, for source LID_390.

were able to find, only through X-ray spectral analysis, nine sources that have the N_H PDF completely above 10^{24} cm^{-2} and the upper boundary pegged at the upper limit of the model adopted $N_H(up) = 10^{26}$ cm^{-2}. Fig. 5 show the spectra and PDF of two such reflection dominated sources, where a very strong Fe Kα line is superimposed to a flat continuum. Most (7/9) of these sources have $z \gtrsim 1.5$, because above these values both the Fe line and the Compton hump are easier to detect.

4 Conclusions

Thanks to the combination of new dedicated models and sophisticated analysis techniques, specifically developed for low counts statistics, recent works have found a growing number of CT AGN at high redshift in deep X-ray surveys (e.g. Brightman et al. 2014, Buchner et al. 2015). We applied a similar approach to the large catalog of X-ray detected AGN in the COSMOS-Legacy survey and demonstrated that not only are mildly CT sources up to $z \sim 3.5$ recoverable via X-ray spectral analysis, but also reflection dominated, heavily CT sources at $z \sim 2$ can be efficiently identified.

We underline, however, that X-rays need to be complemented by rich multiwavelength data, in order to verify that the solution at high N_H - and therefore high L_X - found for each of these sources, is not only statistically motivated, given the available X-ray spectra, but also physically reasonable, given all the other multiwavelength data available.

4.1 Implications for XMM-Newton

While *Chandra* is more efficient in detecting faint (high z and/or obscured) sources[4], the spectra obtained with long *XMM–Newton* exposures have a much higher number of net counts (if the source is bright enough, i.e. few$\times 10^{-15}$ erg cm^{-2} s^{-1}), and they allow to constraint simultaneously the column density, even above 10^{25} cm^{-2} and the reflection fraction, two crucial parameters for CXB models.

As an example we show here the *XMM–Newton* spectrum of source XID-202 in the XMM-CDFS catalog (Ranalli et al. 2013). The nominal 3.4 Ms exposure time invested by *XMM–Newton* (corresponding to an effective exposure time of ~ 6 Ms between pn and MOS1+2) allowed to collect ~ 1500 total net counts (in Fig. 7 we show only the pn spectrum for clarity) for this z=3.7 CT source (Comastri et al. 2011). The spectral quality is high enough to allow us to use a more complex CT model (MYTorus, in the decoupled version) and constraint simultaneously the N_H and the reflection fraction (Fig 7 bottom panel, thick lines). On the other hand, the nominal 4Ms collected with *Chandra* (3.6 effective exposure at the source position) give only

[4] by about a factor $\sim$ 2, as can be derived comparing the total exposure time needed, and the number of CT AGN selected, in the *Chandra* (this work) and *XMM–Newton* (Lanzuisi et al. 2015a) catalogs of a medium/deep survey like COSMOS

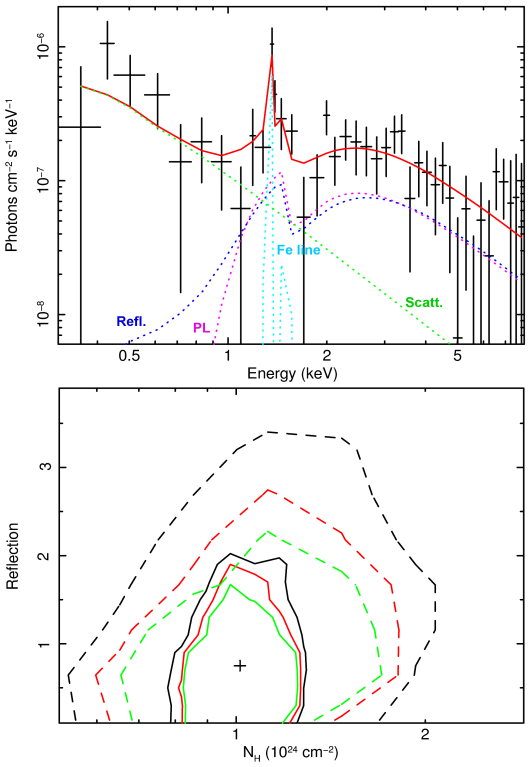

Fig. 7 *Top:* Unfolded spectrum of source XID202 from the XMM-CDFS catalog, a CT AGN at z=3.7. The different components (primary powerlaw, reflection, Fe line complex, scattered emission) are labeled with different colors. *Bottom:* 99, 90 and 68% confidence contours obtained from the *XMM–Newton* spectrum (thick lines) and from the *Chandra* one (dotted lines), for the N_H and reflection fraction.

380 net counts. Despite the much lower background, the uncertainties on these parameters, obtained from the *Chandra* spectrum are much larger (dashed lines).

Of course sources of similar intrinsic luminosity ($L_X > 5 \times 10^{44}$ erg s^{-1}) at high redshift are rare (e.g. Vito et al. 2014). Therefore, the most efficient way to collect a decent sample (e.g. 10 sources) of high redshift CT AGN, at these flux levels ($F_{2-10} \sim 5 \times 10^{-15}$ erg cm^{-2} s^{-1}), for which all the different parameters of a complex CT model can be determined, may be to spend long (e.g. 1Ms) exposure times over CT candidates at high z selected in existing/ongoing large area surveys, such as XMM-XXL (Pierre et al. 2015) or S82 (La Massa et al. 2013).

Acknowledgements. The author acknowledges financial support from the CIG grant "eEASY" n. 321913 and from ASI-INAF grant n. 2014-045-R.0.

References

Akylas, A., Georgakakis, A., Georgantopoulos, I, et al. 2012, A&A, 546, A98
Ballantyne, D. R., Draper, A. R., Madsen, K. K., et al. 2011, ApJ , 736, 56
Brightman, M., & Nandra, K. 2011, MNRAS , 413, 1206
Brightman, M., & Ueda, Y. 2012, MNRAS , 423, 702
Brightman, M., Nandra, K., Salvato, M., et al. 2014, arXiv:1406.4502
Burlon, D., Ajello, M., Greiner, J., et al. 2011, ApJ , 728, 58
Buchner, J., Georgakakis, A., Nandra, K., et al. 2015, ApJ , 802, 89
Cappelluti, N., Brusa, M., Hasinger, G., et al. 2009, A&A, 497, 635
Castelló-Mor, N., Carrera, F. J., Alonso-Herrero, A., et al. 2013, A&A, 556, A114
Civano, F., Elvis, M., Brusa, M., et al. 2012, ApJS , 201, 30
Civano, F., Hickox, R. C., Puccetti, S., et al. 2015, ApJ , 808, 185
Civano, F., Marchesi, S., Comastri, A., et al. 2016, ApJ , 819, 62
Comastri, A., Setti, G., Zamorani, G., & Hasinger, G. 1995, A&A, 296, 1
Comastri, A., Ranalli, P., Iwasawa, K., et al. 2011, A&A, 526, L9
Comastri, A., Gilli, R., Marconi, A., et al. 2015, A&A, 574, L10
Delvecchio, I., Lutz, D., Berta, S., et al. 2015, MNRAS , 449, 373
Elvis, M., Civano, F., Vignali, C., et al. 2009, ApJS , 184, 158
Fiore, F., Grazian, A., Santini, P., et al. 2008, ApJ , 672, 94-101
Gandhi, P., Horst, H., Smette, A., et al. 2009, A&A, 502, 457
Georgantopoulos, I., Dasyra, K. M., Rovilos, E., et al. 2011, A&A, 531, A116
Georgantopoulos, I., Comastri, A., Vignali, C., et al. 2013, A&A, 555, A43
Gilli, R., Comastri, A., & Hasinger, G. 2007, A&A, 463, 79
Gilli, R., Vignali, C., Mignoli, M., et al. 2010, A&A, 519, AA92
Hasinger, G., Cappelluti, N., Brunner, H., et al. 2007, ApJS , 172, 29
Houck, J. R., Soifer, B. T., Weedman, D., et al. 2005, ApJ , 622, L105
Ilbert, O., Capak, P., Salvato, M., et al. 2009, ApJ , 690, 1236
Kormendy, J., & Ho, L. C. 2013, ARA&A , 51, 511
Lacy, M., Storrie-Lombardi, L. J., Sajina, A., et al., 2004, ApJS, 154, 166
Lanzuisi, G., Piconcelli, E., Fiore, F., et al. 2009, A&A, 498, 67
Lanzuisi, G., Civano, F., Elvis, M., et al. 2013, MNRAS , 431, 978
Lanzuisi, G., Ranalli, P., Georgantopoulos, I., et al. 2015a, A&A, 573, AA137 (L15)
Lanzuisi, G., Perna, M., Delvecchio, I., et al. 2015b, A&A, 578, A120
Marchesi, S., Civano, F., Elvis, M., et al. 2016b, ApJ , 817, 34
Marchesi, S., Lanzuisi, G., Civano, F., et al. 2016a, arXiv:1608.05149
Marconi, A., Risaliti, G., Gilli, R., et al. 2004, MNRAS , 351, 169
Martínez-Sansigre, A., Rawlings, S., Lacy, M., et al., 2005, Nature, 436, 666
Murphy, K. D., & Yaqoob, T. 2009, MNRAS , 397, 1549
Mignoli, M., Vignali, C., Gilli, R., et al. 2013, A&A, 556, A29
Ranalli, P., Comastri, A., Vignali, C., et al. 2013, A&A, 555, A42
Risaliti, G., Maiolino, R., & Salvati, M. 1999, ApJ , 522, 157
Salvato, M., Ilbert, O., Hasinger, G., et al. 2011, ApJ , 742, 61
Scoville, N., Aussel, H., Brusa, M., et al. 2007, ApJS , 172, 1
Soltan, A. 1982, MNRAS , 200, 115
Stern, D. 2015, ApJ , 807, 129
Tozzi, P., Gilli, R., Mainieri, V., et al. 2006, A&A, 451, 457
Treister, E., Urry, C. M., & Virani, S. 2009, ApJ , 696, 110
Ueda, Y., Akiyama, M., Hasinger, G., et al. 2014, ApJ , 786, 104
Vignali, C., Alexander, D. M., & Comastri, A. 2006, MNRAS , 373, 321
Vignali, C., Mignoli, M., Gilli, R., et al. 2014, A&A, 571, A34

